quantum teleportation were used as a quantum relay (see Fig. 5) in quantum cryptography, then the probabilistic nature of our teleportation scheme would only affect the count rate, not the quality of the quantum relay. Our scheme would be useful for this application. □

Received 19 September; accepted 13 December 2002; doi:10.1038/nature01376.

1. Bennett, C. H. *et al.* Teleporting an unknown quantum state via dual classical and Einstein-Podolsky-Rosen channels. *Phys. Rev. Lett.* **70,** 1895–1899 (1993).
2. Boschi, D., Branca, S., De Martini, F., Hardy, L. & Popescu, S. Experimental realization of teleporting an unknown pure quantum state via dual classical and Einstein-Podolsky-Rosen channels. *Phys. Rev. Lett.* **80,** 1121–1125 (1998).
3. Bouwmeester, D. *et al.* Experimental quantum teleportation. *Nature* **390,** 575–579 (1997).
4. Nielsen, M. A., Knill, E. & Laflamme, R. Complete quantum teleportation using nuclear magnetic resonance. *Nature* **396,** 52–55 (1998).
5. Kim, Y.-H., Kulik, S. P. & Shih, Y. Quantum teleportation of polarization state with a complete Bell state measurement. *Phys. Rev. Lett.* **86,** 1370–1373 (2001).
6. Lombardi, E., Sciarrino, F., Popescu, S. & De Martini, F. Teleportation of a vacuum–one-photon qubit. *Phys. Rev. Lett.* **88,** 070402 (2002).
7. Jennewein, T., Weihs, G., Pan, J.-W. & Zeilinger, A. Experimental nonlocality proof of quantum teleportation and entanglement swapping. *Phys. Rev. Lett.* **88,** 017903 (2002).
8. Furusawa, A. *et al.* Unconditional quantum teleportation. *Science* **282,** 706–709 (1998).
9. Babichev, S. A., Ries, J., Lvovsky, A. I. Quantum scissors: teleportation of single-mode optical states by mean of a nonlocal single photon. Preprint quant-ph/0208066 at ⟨http://xxx.lanl.gov⟩ (2002).
10. Bowen, W. P. *et al.* Experimental investigation of continuous variable quantum teleportation. Preprint quant-ph/0207179 at ⟨http://xxx.lanl.gov⟩ (2002).
11. Gisin, N., Ribordy, G., Tittel, W. & Zbinden, H. Quantum cryptography. *Rev. Mod. Phys.* **74,** 145–195 (2002).
12. Waks, E., Zeevi, A. & Yamamoto, Y. Security of quantum key distribution with entangled photons against individual attacks. *Phys. Rev A* **65,** 052310 (2002).
13. Jacobs, B. C., Pittman, T. B. & Franson, J. D. Quantum relays and noise suppression using linear optics. *Phys. Rev. A* **66,** 052307 (2002).
14. Gottesman, D. & Chuang, I. L. Demonstrating the viability of universal quantum computation using teleportation and single-qubit operations. *Nature* **402,** 390–393 (1999).
15. Briegel, H.-J., Dur, W., Cirac, J. I. & Zoller, P. Quantum repeaters: The role of imperfect local operations in quantum communication. *Phys. Rev. Lett.* **81,** 5932–5935 (1998).
16. Zukowski, M., Zeilinger, A., Horne, M. A. & Ekert, A. K. "Event-ready-detectors" Bell experiment via entanglement swapping. *Phys. Rev. Lett.* **71,** 4287–4290 (1993).
17. Pan, J.-W., Bouwmeester, D., Weinfurter, H. & Zeilinger, A. Experimental entanglement swapping: Entangling photons that never interacted. *Phys. Rev. Lett.* **80,** 3891–3894 (1998).
18. Lütkenhaus, N., Calsamiglia, J. & Suominen, K.-A. Bell measurements for teleportation. *Phys. Rev. A* **59,** 3295–3300 (1999).
19. Braunstein, S. L. & Kimble, H. J. Teleportation of continuous quantum variables. *Phys. Rev. Lett.* **80,** 869–872 (1998).
20. Tittel, W. & Weihs, G. Photonic entanglement for fundamental tests and quantum communication. *Quant. Inf. Comput.* **1,** 3–56 (2001).
21. Brendel, J., Tittel, W., Zbinden, H. & Gisin, N. Pulsed energy-time entangled twin-photon source for quantum communication. *Phys. Rev. Lett.* **82,** 2594–2597 (1999).
22. Thew, R. T., Tanzilli, S., Tittel, W., Zbinden, H. & Gisin, N. Experimental investigation of the robustness of partially entangled photons over 11 km. *Phys. Rev. A.* **66,** 062304 (2002).
23. De Riedmatten, H., Marcikiç, I., Tittel, W., Zbinden, H. & Gisin, N. Quantum interferences with photon pairs created in spatially separated sources. *Phys. Rev. A* (in the press); preprint quant-ph/0208174 at ⟨http://xxx.lanl.gov⟩ (2002).
24. Marcikic, I., De Riedmatten, H., Tittel, W., Zbinden, H. & Gisin, N. Femtosecond time-bin entangled qubits for quantum communication. *Phys. Rev. A* **66,** 062308 (2002).
25. Lamas-Linares, A., Howell, J. C. & Bouwmeester, D. Stimulated emission of polarization-entangled photons. *Nature* **412,** 887–890 (2001).
26. Owens, P. C. M., Rarity, J. G., Tapster, P. R., Knight, D. & Townsend, P. D. Photon counting with passively quenched germanium avalanche. *Appl. Opt.* **33,** 6895–6901 (1994).
27. Stucki, D., Ribordy, G., Stefanov, A. & Zbinden, H. Photon counting for quantum key distribution with Peltier cooled InGaAs/InP APD's. *J. Mod. Opt.* **48,** 1967–1981 (2001).
28. Massar, S. & Popescu, S. Optimal extraction of information from finite quantum ensembles. *Phys. Rev. Lett.* **74,** 1259–1263 (1995).
29. Tittel, W., Brendel, J., Zbinden, H. & Gisin, N. Quantum cryptography using entangled photons in energy-time Bell states. *Phys. Rev. Lett.* **84,** 4737–4740 (2000).
30. De Riedmatten, H., Marcikic, I., Zbinden, H. & Gisin, N. Creating high dimensional entanglement using mode-locked laser. *Quant. Inf. Comput.* **2,** 425–433 (2002).
31. Grangier, P., Levenson, J. A. & Poizat, J.-P. Quantum non-demolition measurements in optics. *Nature* **396,** 537–542 (1998).

Acknowledgements We thank M. Legré for discussions, and C. Barreiro and J.-D. Gautier for technical support. Financial support by the Swiss OFES and NSF within the framework of the European IST project Qucomm and the Swiss National Center for Quantum Photonics is acknowledged. W.T. acknowledges support from the ESF Programme Quantum Information Theory and Quantum Computation (QIT).

Competing interests statement The authors declare that they have no competing financial interests.

Correspondence and requests for materials should be addressed to N.G. (e-mail: Nicolas.Gisin@Physics.Unige.ch).

A colloidal model system with an interaction tunable from hard sphere to soft and dipolar

Anand Yethiraj*† **& Alfons van Blaaderen***

* *Soft Condensed Matter, Debye Institute, Utrecht University, Padualaan 5, 3584CC Utrecht, and FOM Institute for Atomic and Molecular Physics, Kruislaan 407, 1098 SJ Amsterdam, The Netherlands*

Monodisperse colloidal suspensions of micrometre-sized spheres are playing an increasingly important role as model systems to study, in real space, a variety of phenomena in condensed matter physics—such as glass transitions and crystal nucleation[1–4]. But to date, no quantitative real-space studies have been performed on crystal melting, or have investigated systems with long-range repulsive potentials. Here we demonstrate a charge- and sterically stabilized colloidal suspension—poly(methyl methacrylate) spheres in a mixture of cycloheptyl (or cyclohexyl) bromide and decalin—where both the repulsive range and the anisotropy of the interparticle interaction potential can be controlled. This combination of two independent tuning parameters gives rise to a rich phase behaviour, with several unusual colloidal (liquid) crystalline phases, which we explore in real space by confocal microscopy. The softness of the interaction is tuned in this colloidal suspension by varying the solvent salt concentration; the anisotropic (dipolar) contribution to the interaction potential can be independently controlled with an external electric field ranging from a small perturbation to the point where it completely determines the phase behaviour. We also demonstrate that the electric field can be used as a pseudo-thermodynamic temperature switch to enable real-space studies of melting transitions. We expect studies of this colloidal model system to contribute to our understanding of, for example, electro- and magneto-rheological fluids.

Recent advances in quantitative three-dimensional (3D) real-space analysis of the structure and dynamics of colloids have been accompanied by progress in the synthesis of model spheres with a controllable size and surface chemistry enabling the manipulation of the interaction potentials between the spheres[5,6]. Together with the well developed scattering techniques for studying colloidal systems[7–12], this has led to new insights into the glass transition of simple glass formers[2,3,12,13], crystal nucleation and growth[4,7–10,14], and the role of the attractive part of interaction potentials on phase behaviour[11].

The simplest colloidal model system with short-ranged repulsive interactions is either a sterically stabilized particle suspension[5,14,15], or an aqueous suspension of micrometre-sized latex spheres with salt added to ensure that the inverse Debye screening length, $1/\kappa$, a measure for the range of the repulsion, is short; $\kappa R = 33$ for spheres of radius $R = 1\,\mu$m in water at a monovalent salt concentration of $c = 0.1$ mM. To realize almost hard-sphere behaviour, the always-present van der Waals attractions have to be reduced by matching the index of refraction in the visible. This allows the interactions to be tuned to almost hard-sphere-like even for micrometre-sized colloids that can be quantitatively imaged in 3D by confocal microscopy. The role of gravity (far more important in colloids than in the crystallization of atomic and molecular fluids) is minimized by matching the density of the spheres and solvent. A step-up in complexity could involve either introducing a dipolar interaction, thus making the interaction anisotropic, or extending

† Present address: Department of Chemistry, 2036 Main Mall, Vancouver, British Columbia, Canada V6T 1Z1.

the range of the repulsion (for example, increasing the screening length $1/\kappa$ such that $\kappa R \approx 1$). The latter can be achieved in aqueous suspensions by removing ions by using ion-exchange resin, but it is difficult to reduce concentrations below 1 μM (that is, $1/\kappa \approx 300$ nm). We will show that in less polar organic solvents, screening lengths of $1/\kappa \approx 12$ μm can be achieved. Dipolar interactions are induced, and finely controlled via an external electric field (the 'electrorheological effect'[16]). Studies of structure evolution in brownian hard-sphere fluids with an added dipolar interaction[17–20] show the formation of strings, then sheets and finally 3D crystallites. As far as we know, long-range repulsive colloidal spheres with anisotropic interactions have not yet been studied.

Here we present confocal microscopy studies of charged and sterically stabilized polymethyl methacrylate (PMMA) spheres (radius $R = 1.0$ and 2.0 μm) in a density- and refractive-index-matched organic solvent mixture; this mixture polar enough (dielectric constant, $\varepsilon = 5$–6) to have electric-field-induced dipolar interactions. Two solvent mixtures were used: cycloheptyl bromide/*cis*-decalin and cyclohexyl bromide/*cis*-decalin. The PMMA spheres were monodisperse, fluorescently labelled and sterically stabilized[5,21]. Three-dimensional particle coordinates of the colloids were obtained as described before[2,3]. Charge on PMMA spheres in similar solvent mixtures to those used here was previously reported to result from the presence of water or from the dye incorporated in the particles[4,22]. However, we found that neither drying and distilling the cycloheptyl bromide, nor the use of undyed particles, had an effect on the softness of the potential. We found that we could control the range of the repulsive interactions by adding the salt tetrabutylammonium chloride.

Hard-sphere suspensions are fluid at low particle volume fractions φ but crystallize into a close-packed crystal structure for $\varphi > 0.545$. A random hexagonal close packing (r.h.c.p.) is observed experimentally, as opposed to the theoretically predicted face-centred cubic (f.c.c.) crystal[23]. When the potential is made soft (κR smaller), crystallization occurs for smaller φ. The crystal structure is then f.c.c. although for a range of κR values, there can be an intervening body-centred cubic (b.c.c.) phase. The phase behaviour has been extensively studied[9,24–26], and modelled (and reproduced, with a renormalized surface charge density[26]) by a pure Yukawa[24] or a hard-sphere-plus-Yukawa[27] potential. In Fig. 1a–c, we demonstrate the fine control of the softness of the interparticle interaction. Samples in Fig. 1a and b were prepared at identical volume fraction $\varphi = 0.02$. The sample in Fig. 1a ($c = 40$ μM) was fluid, while that in Fig. 1b, in a pure suspension without added salt (corresponding to $1/\kappa \approx 12$ μm) was crystalline. The system shown in Fig. 1c, also in the pure suspension, was crystalline at $\varphi = 0.002$. At $c = 260$ μM the inter-particle spacing was $\sigma/2R = 1.16 \pm 0.01$,

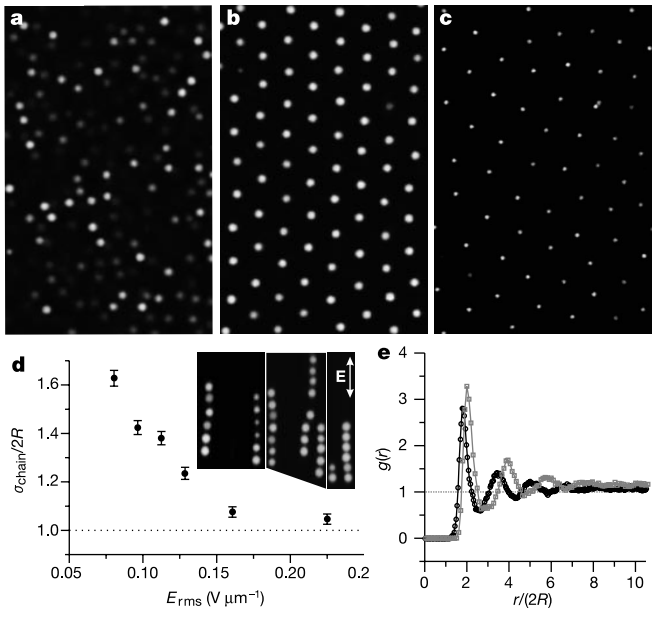

Figure 1 Tunability of interactions. Spheres, radius $R = 2.0$ μm; suspension medium, cyclohexyl bromide-*cis*-decalin. **a**, Fluid at volume fraction $\varphi = 0.02$, salt concentration $c = 40$ μM, maximum of first peak in 2D pair correlation function $g(r)$, 8.0 μm. **b**, Crystalline (f.c.c.) at $\varphi = 0.02$ and no salt, interparticle spacing, 11.7 μm. **a**, **b**, Confocal micrographs of 2D snapshots 50 μm into the sample bulk. **c**, $\varphi = 0.002$ (no salt). A plane 33 μm above the bottom surface is shown: the interparticle spacing $\sigma \approx 26.7$ μm. **d**, The string interparticle spacing σ_{chain} decreases with increasing field, owing to a balance between anisotropic attraction and charge repulsion. Inset, a 1-MHz a.c. external field $E_{rms} = 0.09$, 0.14 and 0.25 V μm^{-1} respectively; field direction, z as shown) induces the formation of strings. At fields above $E_{rms} = 0.35$ V μm^{-1}, the strings span the sample so there is 1D periodicity. **e**, In the x-y plane, however, the suspension remains fluid-like. Shown is 2D $g(r)$ at zero-field (black circles) and $E_{rms} = 0.35$ V μm^{-1} (grey squares). The structure in both cases is liquid-like: however the peaks in the 'string fluid' are shifted farther out, and higher due to the in-plane registry caused by the 1D periodicity.

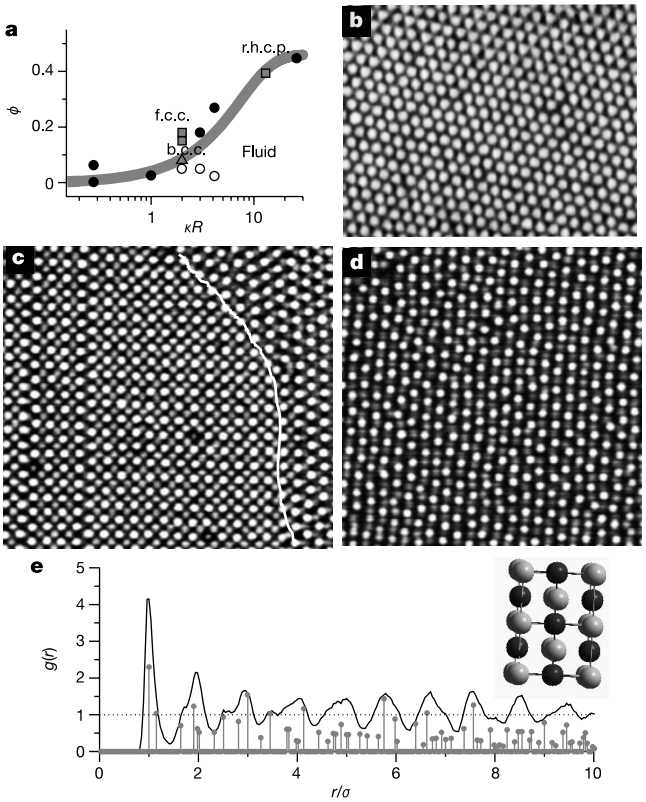

Figure 2 Influence of softness on the phase behaviour. **a**, Phase diagram as function of softness, κR ($1/\kappa$ is the inverse Debye screening length). The grey triangle (b.c.c.) and squares (f.c.c.) are data for 1-μm spheres in cycloheptyl bromide-*cis*-decalin; (pure and at $c = 260$ μM); the circles are for 2-μm spheres in cyclohexyl bromide-*cis*-decalin, pure and $c = 10$–260 μM. Open circles are fluid and closed circles are solid close to fluid–solid coexistence. Thick grey line is our best estimate of the phase boundary. **b**–**d**, x–y confocal images of: **b**, hexagonal plane in r.h.c.p crystal; **c**, (100) face of f.c.c. (left) crystal coexisting with a (111) oriented f.c.c. (right); drawn in white is a grain boundary. **d**, (110) face (not a hexagonal plane) of b.c.c. crystal. **e**, Crystal structures are quantified by the in-plane pair correlation function $g(r)$ (plotted against r/σ where $\sigma \neq 2R$ is the mean interparticle spacing) and direct measurement of interplane stacking and separations. 2D $g(r)$ of b.c.c. (110) face (solid black line is experiment, grey vertical lines are calculated). Inset, a model of the b.c.c. (110) face. Grey and black circles denote different planes.

corresponding to $\varphi = 0.42$–0.45 at crystallization, which is hard-sphere-like (Fig. 2b) and close to the system reported in previous studies[4,14]. The Debye lengths were estimated from conductivity measurements, implying a degree of salt dissociation of $<1\%$; electrophoresis measurements gave an estimate of $\zeta = +100\,\mathrm{mV} \approx 4k_BT/e$ for the surface potential (here k_B is Boltzmann's constant, T is temperature and e is the charge on the electron). We independently quantified the softness by the position of the first peak of the two-dimensional (2D) pair correlation function $g(r)$ as function of added salt at different values of φ, close to the fluid–solid phase boundary (see Methods for details).

The disorder–order phase diagram (Fig. 2a) as a function of κR and φ is illustrated by 2D planes from an r.h.c.p., f.c.c. and b.c.c. crystal (Fig. 2b, c and d, respectively). Samples with a linear concentration gradient (see Methods section for details) were used to map out phase boundaries. We then prepared homogeneous samples at volume fractions close to the phase boundary for a more quantitative analysis. A transition from a soft to a hard-sphere regime was observed (and quantified—see, for example, the analysis for the b.c.c. crystal in Fig. 2e). At $\kappa R \approx 0.3$, we obtained a 'solid' with a lattice spacing of $\approx$27 μm (Fig. 1c). At $\kappa R \approx 2$ we observed a fluid-to b.c.c.-to-f.c.c. phase sequence with increasing volume fraction, while at $\kappa R \approx 13$ and 26 a hard-sphere-like fluid-to-r.h.c.p. phase sequence was observed. Figure 1d shows the effect of the second deviation from hard-sphere-like, namely anisotropy. The electric field (along z in Fig. 1d, inset) caused the spheres to chain into strings along z. The average sphere–sphere spacing, σ_{chain}, in the string (obtained from a 2D autocorrelation of each xz snapshot) decreased (Fig. 1d) with increasing field, saturating when $(\sigma_{chain} - 2R)/2 = 100\,\mathrm{nm}$, a distance which is close to our estimate of the inverse-Debye length in the hard-sphere-like suspensions ($1/\kappa \approx 76\,\mathrm{nm}$). Fig. 1e shows $g(r)$ for a 2D snapshot in a 3D fluid and in a string fluid. Whereas the strings (such as shown in Fig. 1d inset) had one-dimensional order along z, the 2D plane perpendicular to z was fluid-like, although with a stronger repulsion than in a normal fluid: the peak was higher and further from the origin.

We explored (Fig. 3) the phase diagram of the dipolar soft ($\kappa R \approx 2$) spheres (DP-SS) in the volume fraction–electric field plane. At low and zero electric fields, we observed a fluid-b.c.c.-f.c.c. phase sequence (with the b.c.c. phase existing for $0.08 < \varphi < 0.15$). The existence of the b.c.c. phase at volume fractions as high as $\varphi \approx 0.15$, although also observed in an X-ray scattering study of the phase diagram in an aqueous system[25] (also at comparable κR), and even feasible theoretically[27], is not expected for $\zeta/(k_BT/e) = 4$. For $0.08\,\mathrm{V\,\mu m^{-1}} < E_{rms} < 0.35\,\mathrm{V\,\mu m^{-1}}$, where E_{rms} is the root-mean-square electric field, strings were observed with a distribution of string lengths and monotonic-decreasing sphere separation (Fig. 1d and inset). At $E_{rms} = 0.35\,\mathrm{V\,\mu m^{-1}}$, with strings spanning the electrodes (and $(\sigma_{chain} - 2R)/2 = 100\,\mathrm{nm}$), the 'string-fluid' was the stable phase for $\varphi < 0.15$. The long-range repulsion stabilized individual strings. It appears over the duration of our experiment (up to several hours) to be an equilibrium phase, with, as expected, the dynamics of the strings (Fig. 3e) being significantly slower (diffusion coefficient $D \approx 0.45(\mu m)^2\ \mathrm{min}^{-1}$) than that of the individual spheres in the corresponding zero-field fluid phase. This is in sharp contrast with the dipolar hard-sphere (DP-HS) case, where strings form owing to the dipolar interaction but 'zip up' into sheets within a few milliseconds[20]. The sheets

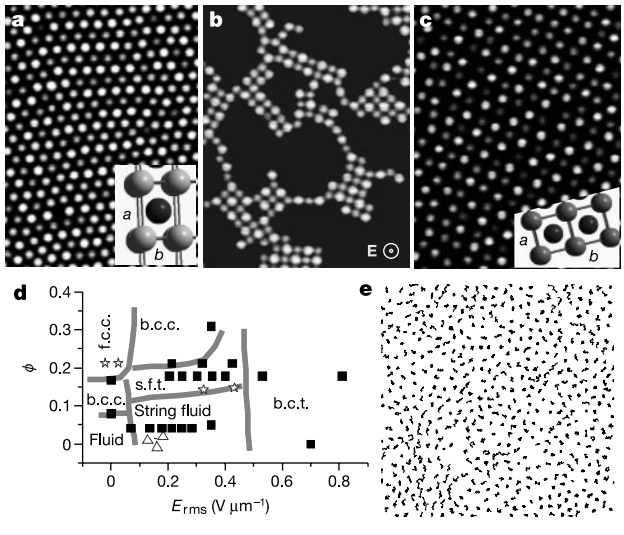

Figure 3 Volume fraction–electric field phase diagram. Data are for 1-μm spheres in cycloheptyl bromide-*cis*-decalin, no salt added. **a**–**c**, *x*-*y* confocal images of **a**, body-centred orthorhombic (b.c.o.) ($c = 2.187\,\mu m$; $b = 1.244c$; $a = 1.97c$, model in inset), **b**, body-centred tetragonal (b.c.t.) ($a = b = 2.44\,\mu m$; $c = 2.0\,\mu m$, $a/c = 1.22$: ratio a/c for b.c.t. is theoretically $\sqrt{3/2} = 1.2247$), and **c**, space-filling tetragonal (s.f.t.) crystal ($c = 2.0\,\mu m$; $a = b$; $a/c = 1.846$, model in inset). **d**, The phase diagram. Grey lines indicate approximate phase boundaries, open stars two-phase coexistence, and open triangles are in the string fluid with a distribution of lengths of string that do not span the electrodes. The solid squares are all points where *xyt* or *xyz* data stacks were taken. **e**, Trajectory (time step, 30 s) of strings (ordered along z) diffusing in the *x*–*y* plane.

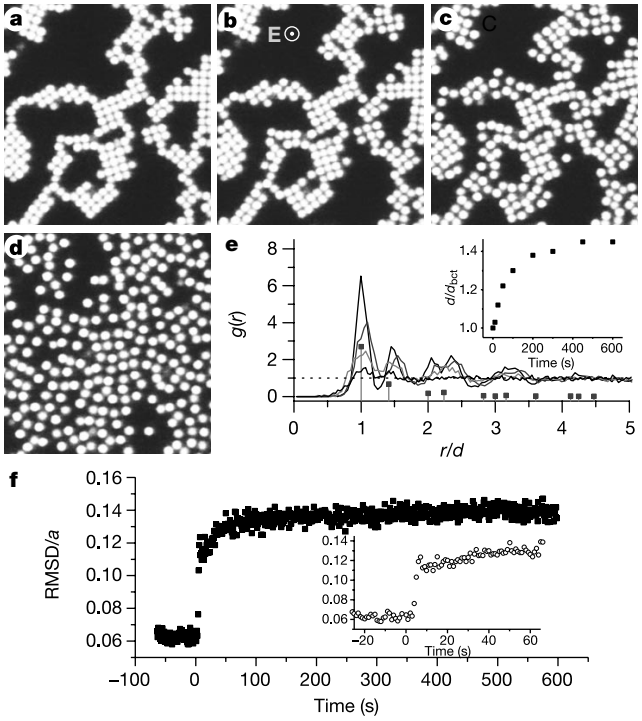

Figure 4 Melting of a b.c.t. crystal into a string fluid is not the reverse of crystallization of the string fluid. This quasi-2D transition is shown qualitatively in images taken at times $t = 0$ (**a**), 10 s (**b**), 50 s (**c**) and 600 s (**d**). The polycrystalline b.c.t. phase melts into a tetragonal crystal with larger in-plane lattice spacings: this crystal is metastable for several seconds. **e**, The $g(r)$ of two projected planes (which contain all the information in a unit cell) shows peaks characteristic of the initial four-fold symmetric lattice (grey vertical lines are calculated positions for a square lattice). Pair correlations at later times fall within the envelope of that at $t = 0$ s provided that the distances are rescaled by a numerical factor that increases in time until it reaches the value for the peak position in the string fluid (inset). **f**, The scaled root-mean-square deviation (RMSD/a) versus time; RMSD/a is scaled with respect to the in-plane lattice constant ($a = b$) because the out-of-plane fluctuations are negligible. Within $t = 10$ s (see inset), RMSD/a increases from 0.06 to 0.12, and at long times saturates at 0.14.

too are short-lived dynamical structures that coarsen into three-dimensional b.c.t. ($a = b = c\sqrt{3/2}$) crystallites. We reproduced this DP-HS limit in a test sample of 1-μm spheres in cycloheptyl bromide/*cis*-decalin at $c = 260\,\mu M$, where we indeed observed a direct transition from fluid to (non-space-filling, $a = b = c\sqrt{3/2}$) b.c.t. crystallites with no intervening phase at intermediate fields.

Peculiar to DP-SS is an intermediate field regime with qualitatively different physics, and new crystal structures that arise purely from the competition of the soft repulsion and the anisotropic dipolar interaction. At $\phi \approx 0.25$ the string fluid crystallized to form a space-filling tetragonal (s.f.t.) solid phase (Fig. 3c), where (unlike the b.c.t. phase) the $a = b$ lattice vectors are such as to fill space, with $c \approx 2R$. Hence we observed, not several crystallites with the solvent continuum between them, but a single polycrystalline tetragonal solid. In order to distinguish the two, we use the terms s.f.t. and b.c.t. although in principle both structures are body-centred tetragonal. At $\varphi > 0.30$, we observed (Fig. 3a) a body-centred orthogonal (b.c.o.) crystal structure $c \approx 2R \neq a \neq b$. Indeed there was a reversible transition from b.c.o. to s.f.t. as the field was increased at ($\varphi = 0.21$, $E_{rms} = 0.32\,V\,\mu m^{-1}$). At high electric fields ($E_{rms} = 0.7\,V\,\mu m^{-1}$), we observed (Fig. 3b) b.c.t. crystallites with $a = b = c\sqrt{3/2}$, with $c \approx 2R$ as in the DP-HS case[20].

We can understand the physical processes at intermediate fields as follows. At low fields, charge repulsion dominates, whereas at high field, the anisotropic dipolar interaction (which is attractive along the field direction) predominates. At intermediate fields, attractions dominate along the field direction, while repulsion dominates in the plane perpendicular to this direction. Even in the DP-HS case, the attraction of two strings is only favoured when thermal fluctuations allow string undulations: in the absence of thermal fluctuations, the string–string interaction would decay exponentially[28]. In the DP-SS case at intermediate fields, charge repulsion in the lateral plane dominates the weaker fluctuation effects.

Finally, we used the electric field as a surrogate temperature field to follow the dynamics of melting of a b.c.t. crystal into a string-fluid phase close to the string-fluid–s.f.t. phase boundary ($\varphi = 0.1$). On increasing the field, the string fluid crystallized into b.c.t. ($a = b = 2R\sqrt{3/2}$). On lowering the field, we saw the sequence shown in Fig. 4. Figure 4a shows the b.c.t. when the field was reduced from $E_{rms} = 0.53\,V\,\mu m^{-1}$ to $0.35\,V\,\mu m^{-1}$. At $t = 10$ s and 25 s, there was still crystallinity with four-fold symmetry (as shown in Fig. 4e where the $g(r)$ is plotted for all the times shown in the images, and compared with the peaks expected for a perfect square lattice), which decreased in time. Finally at $t = 600$ s, the structure was almost liquid-like. Note that in Fig. 4e, the distance is rescaled such that the first peak is unity. This rescaling factor (see inset) was $d = d_{bct} = (\sqrt{3}/2)(2R)$ for a projection of two consecutive (001) b.c.t. planes, but increased with time until it saturates at the string-fluid value. The four-fold symmetric $g(r)$ persisted with this larger transverse length scale for more than 25 s. We also computed a dynamical order parameter, the average root-mean-square deviation (RMSD/a, scaled with respect to the in-plane lattice constant; Fig. 4f) of particle positions between two successive images in the time series. Here, within $t = 10$ s, RMSD/a increased from 0.06 to 0.12, and at long times saturated at 0.14. Thus the b.c.t. phase melted quickly ($t < 10$ s), but the equilibrium string-fluid phase was preceded by a transient s.f.t. structure that persisted for minutes.

The present system significantly extends the use of colloids as condensed matter model systems. The system is refractive-index and density matched, so that bulk measurements in real-space are possible. In the intermediate-field regime of the phase diagram where both softness and anisotropy are important, we observed three colloidal phases composed of repelling strings. Long-ranged repulsive spheres are being used in new photonic applications[29], and dipolar interactions in electro-rheological fluids. We expect that the phases we report here, together with the increased control over interparticle interactions, that is now possible, will lead to important extensions of these and other advanced materials. □

Methods

Sample preparation

Special precautions need to be taken when using low-ionic-strength non-aqueous suspensions. The cyclohexyl bromide ('CH6B'), cycloheptyl bromide ('CH7B') and *cis*-decalin ('CD') were obtained from Sigma-Aldrich. The cycloheptyl and hexyl bromides had a yellowish colour (as bought), and were dried first and then vacuum-distilled, resulting in a colourless liquid. The *cis*-decalin was used as bought. The solutions of tetrabutylammonium chloride ('TBAC'; Sigma-Aldrich) in CH6B or CH7B were prepared by dilution from a stock solution which was close to the saturation concentration at room temperature (293 K) and pressure.

Transient charging effects caused by tribo-electricity can have relaxation times of the order of minutes, so particle suspensions were allowed to stand for hours to be sure they were in equilibrium. Moreover, we could eliminate static charging effects by using indium tin oxide/(ITO)-coated electrodes, and shorting and grounding both electrodes to be sure that the electric field was truly zero. In the experiments reported here, we imaged primarily at low intensities (the 488 nm line of the Ar/Kr mixed gas laser at $<200\,\mu W$) to make sure the self-dissociation of the liquid was not influenced by the light. We used both rectangular glass capillaries and sandwich ITO glass cells.

Electrical conductivity measurements

We measured the electric conductivity (WTW InoLab Level 1, with LR325/01 conductivity cell; cell constant $0.100\,cm^{-1}$) of pure CH6B-CD (and CH7B-CD) and for salt concentrations $c = 10$–$260\,\mu M$. Although the conductivity in the pure solvent mixture at all particle concentrations was too low ($<0.02\,\mu S\,cm^{-1}$) to measure, we could measure conductivities with salt added. For these values we may then estimate the ionic strength c_i using Walden's rule ($\Lambda_0^{water}\eta_0^{water} = \Lambda_0\eta_0$, where Λ_0, η_0, and Λ_0^{water}, η_0^{water} are the limiting molar conductivity and solvent viscosity in the solvent of interest and in water, respectively), $c_i = K/(10^3\Lambda_0)$, K being the electrical conductivity, and thereby the Debye length $\kappa^{-1} = 0.034\sqrt{\varepsilon/c_i}$. For example, at salt concentration $c = 260\,\mu M$ (by weighing) we obtained an ionic strength $c_i = 1.2\,\mu M$ giving an inverse Debye length of 76 nm. The degree of salt dissociation is thus $c_i/c \approx 0.5\%$.

Electrophoretic mobility measurements

To further quantify the softness, we measured the electrophoretic mobility via electrophoretic light scattering (Coulter Delsa 440SX) in a density-matched but highly scattering solvent mixture (CH6B-*n*-hexane), which exhibits similar charged behaviour: owing to the low electrical conductivity in the zero-salt solvent mixture, this was done only at $c_i \approx 0.2\,\mu M$. In this case we obtained a mobility of $0.37\,\mu m\,cm\,V^{-1}\,s^{-1}$ which yields (via the O'Brien and White numerical scheme[30]) $\zeta \approx 4k_BT/e$, a rather large and positive surface potential. Given that the inverse Debye length obtained is a lower bound, the ζ value is a lower bound as well.

Phase boundary determination

Phase boundaries were first mapped out using concentration gradient samples. Such samples were made by filling half of a 100-μm-thick capillary with suspension at large φ, then the other half at low φ, sealing, allowing to equilibrate for several days, and looking closely at the interfacial region. Another way of accessing concentration gradients very quickly was to look at the sedimentation profile in imperfectly density-matched suspensions. The interparticle spacing at the fluid–solid interface gave us a rough but dependable estimate of φ. Via confocal microscopy we obtained 2D slices in the sample bulk, which we used to calculate the 2D pair correlation function $g(r)$ (for example, Figs 1e and 2e). The position of the first peak of the pair-correlation function was an independent determinant of the crystallization volume fraction at the fluid–solid phase boundary, and therefore an independent quantifier of the interaction softness.

Received 15 August; accepted 19 November 2002; doi:10.1038/nature01328.

1. Grier, D. G. & Murray, C. A. The microscopic dynamics of freezing in supercooled colloidal fluids. *J. Chem. Phys.* **100,** 9088–9095 (1994).
2. van Blaaderen, A. & Wiltzius, P. Real-space structure of colloidal hard-sphere glasses. *Science* **270,** 1177–1179 (1995).
3. Kegel, W. K. & van Blaaderen, A. Direct observation of dynamical heterogeneities in colloidal hard-sphere suspensions. *Science* **287,** 290–293 (2000).
4. Gasser, U., Weeks, E. R., Schofield, A., Pusey, P. N. & Weitz, D. A. Real-space imaging of nucleation and growth in colloidal crystallization. *Science* **292,** 258–262 (2001).
5. Antl, L., Goodwin, J., Hill, R., Ottewill, R. & Waters, J. The preparation of poly(methyl methacrylate) latices in non-aqueous media. *Colloids Surf.* **17,** 67–78 (1986).
6. van Blaaderen, A. & Vrij, A. Synthesis and characterization of colloidal dispersions of fluorescent, monodisperse silica spheres. *Langmuir* **8,** 2921–2931 (1992).
7. Dhont, J. K. G., Smits, C. & Lekkerkerker, H. N. W. A time resolved static light-scattering study on nucleation and crystallization in a colloidal system. *J. Colloid Interf. Sci.* **152,** 386–401 (1992).
8. Russel, W. B., Chaikin, P. M., Zhu, J., Meyer, W. V. & Rogers, R. Dendritic growth of hard sphere crystals. *Langmuir* **13,** 3871–3881 (1997).
9. Palberg, T. Crystallization kinetics of repulsive colloidal spheres. *J. Phys. Condens. Matter* **11,** R323–R360 (1999).
10. Harland, J. L. & vanMegen, W. Crystallization kinetics of suspensions of hard colloidal spheres. *Phys. Rev. E* **55,** 3054–3067 (1997).
11. Gast, A. P. & Russel, W. B. Simple ordering in complex fluids—Colloidal particles suspended in solution provide intriguing models for studying phase transitions. *Phys. Today* **51,** 24–30 (1998).

12. Pham, K. N. *et al.* Multiple glassy states in a simple model system. *Science* **269,** 104–106 (2002).
13. Weeks, E. R., Crocker, J. C., Levitt, A. C., Schofield, A. & Weitz, D. A. Three-dimensional direct imaging of structural relaxation near the colloidal glass transition. *Science* **287,** 627–631 (2000).
14. Pusey, P. N. & van Megen, W. Phase behaviour of concentrated suspensions of nearly hard colloidal spheres. *Nature* **320,** 340–342 (1986).
15. Russel, W. B., Schowalter, W. R. & Saville, D. A. *Colloidal Dispersions* (Cambridge Univ. Press, Cambridge, 1999).
16. Parthasarathy, M. & Klingenberg, D. J. Electrorheology: mechanisms and models. *Mater. Sci. Eng.* **R17,** 57–103 (1996).
17. Tao, R. & Jiang, Q. Simulation of structure formation in an electrorheological fluid. *Phys. Rev. Lett.* **73,** 205–208 (1994).
18. Martin, J. E., Odinek, J. & Halsey, T. C. Evolution of structure in a quiescent electrorheological fluid. *Phys. Rev. Lett.* **69,** 1524–1527 (1992).
19. Martin, J. E., Anderson, R. A. & Tigges, C. P. Simulation of the athermal coarsening of composites structured by a uniaxial field. *J. Chem. Phys.* **108,** 3765–3787 (1998).
20. Dassanayake, U., Fraden, S. & van Blaaderen, A. Structure of electrorheological fluids. *J. Chem. Phys.* **112,** 3851–3858 (2000).
21. Bosma, G. *et al.* Preparation of monodisperse, fluorescent PMMA-latex colloids by dispersion polymerization. *J. Colloid Interf. Sci.* **245,** 292–300 (2002).
22. de Hoog, E. H. A., Kegel, W. K., van Blaaderen, A. & Lekkerkerker, H. N. W. Direct observation of crystallization and aggregation in a phase-separating colloid-polymer suspension. *Phys. Rev. E* **64,** 021407 (2001).
23. Pronk, S. & Frenkel, D. Can stacking faults in hard-sphere crystals anneal out spontaneously? *J. Chem. Phys.* **110,** 4589–4592 (1999).
24. Robbins, M. O., Kremer, K. & Grest, G. S. Phase diagram and dynamics of Yukawa systems. *J. Chem. Phys.* **88,** 3286–3312 (1988).
25. Sirota, E. B. *et al.* Complete phase-diagram of a charged colloidal system - A synchrotron X-ray scattering study. *Phys. Rev. Lett.* **62,** 1524–1527 (1989).
26. Monovoukas, Y. & Gast, A. P. The experimental phase diagram of charged colloidal suspensions. *J. Colloid Interf. Sci.* **128,** 533–548 (1989).
27. El Azhar, F., Baus, M., Ryckaert, J.-P. & Meijer, E. J. Line of triple points for the hard-core Yukawa model: A computer simulation study. **112**, 5121–5126 (2000).
28. Halsey, T. C. & Toor, W. Structure of electrorheological fluids. *Phys. Rev. Lett.* **65,** 2820–2823 (1990).
29. Holtz, J. H. & Asher, S. A. Polymerized colloidal crysal hydrogel films as intelligent chemical sensing materials. *Nature* **389,** 829–832 (1997).
30. O'Brien, R. W. & White, L. R. Electrophoretic mobility of a spherical colloidal particle. *J. Chem. Soc. Faraday Trans. II* **74,** 1607–1626 (1978).

Acknowledgements We thank G. Bosma for particle synthesis, C. van Kats for electrophoresis measurements, H. Wisman for technical support, K. van Walree for the suggestion of TCAB salt, and discussion of charge mechanisms, and J. Hoogenboom, S. Auer and D. Frenkel for discussion. We also thank M. Dijkstra and G. Patey for a critical reading of the manuscript. This work is part of the research program of the 'Stichting voor Fundamenteel Onderzoek der Materie (FOM)', which is financially supported by the 'Nederlandse organisatie voor Wetenschappelijke Onderzoek (NWO)'.

Competing interests statement The authors declare that they have no competing financial interests.

Correspondence and requests for materials should be addressed to A.Y. (e-mail: yethiraj@chem.ubc.ca) or A.v.B. (e-mail: A.vanBlaaderen@phys.uu.nl).

High-temperature superconductor bulk magnets that can trap magnetic fields of over 17 tesla at 29 K

Masaru Tomita*† & Masato Murakami*

** Superconductivity Research Laboratory, Shibaura 1-16-25, Minato-ku, Tokyo 105-0023, Japan*
† Railway Technical Research Institute, 2-8-38 Hikari-cho, Kokubunji-shi, Tokyo 185-8540, Japan

Large-grain high-temperature superconductors of the form RE-Ba-Cu-O (where RE is a rare-earth element) can trap magnetic fields of several tesla at low temperatures, and so can be used for permanent magnet applications[1,2]. The magnitude of the trapped field is proportional to the critical current density and the volume of the superconductor[3,4]. Various potential engineering applications for such magnets have emerged[5–13], and some have already been commercialized[7–10]. However, the range of applications is limited by poor mechanical stability and low thermal conductivity of the bulk superconductors[14–17]; RE-Ba-Cu-O magnets have been found to fracture during high-field activation, owing to magnetic pressure[14–16]. Here we present a post-fabrication treatment that improves the mechanical properties as well as thermal conductivity of a bulk Y-Ba-Cu-O magnet, thereby increasing its field-trapping capacity. First, resin impregnation and wrapping the materials in carbon fibre improves the mechanical properties. Second, a small hole drilled into the centre of the magnet allows impregnation of Bi-Pb-Sn-Cd alloy into the superconductor and inclusion of an aluminium wire support, which results in a significant enhancement of thermal stability and internal mechanical strength. As a result, 17.24 T could be trapped, without fracturing, in a bulk Y-Ba-Cu-O sample of 2.65 cm diameter at 29 K.

Bulk RE-Ba-Cu-O superconductors have a complex structure, consisting of an $REBa_2Cu_3O_y$ matrix in which are distributed small particles of RE_2BaCuO_5. $REBa_2Cu_3O_y$ materials undergo the tetragonal to orthorhombic transformation, which causes crystal deformation. During this transformation the crystal takes up oxygen, and as a result the *c* axis shrinks, leading to the formation of microcracks perpendicular to this axis[18]. In addition, when the RE-Ba-Cu-O precursors melt, oxygen gas is released from the crystal; some of this gas remains in the sample (because of high viscosity), resulting in the formation of microvoids[19]. These defects are difficult to elim-

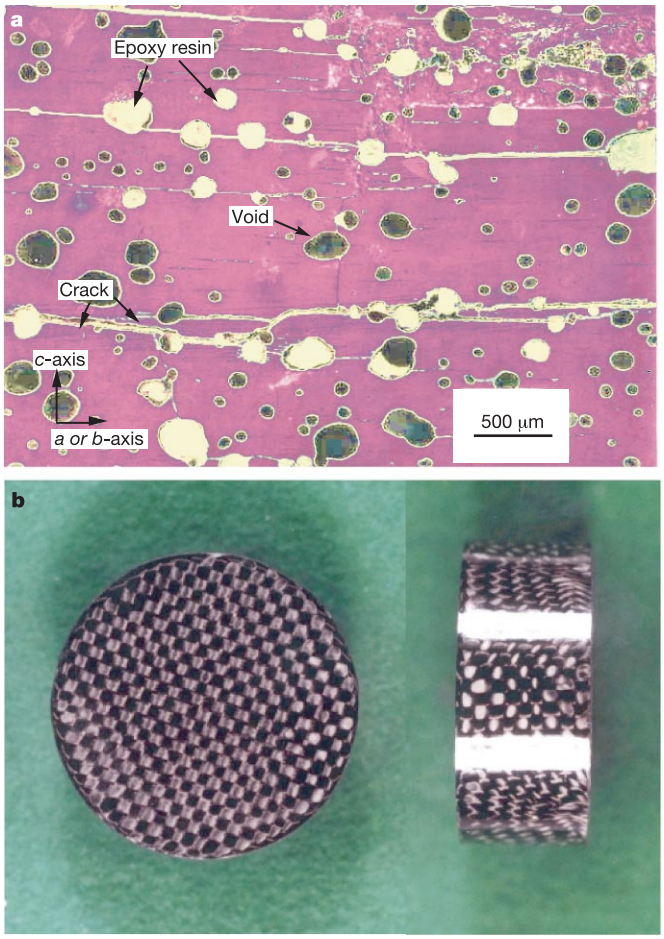

Figure 1 Resin-impregnated Y-Ba-Cu-O with carbon fibre wrapping. **a**, Cross-sectional view of a resin-impregnated Y-Ba-Cu-O (YBCO) disk. Note that resin penetrates through the surface cracks, and fills cracks and voids inside the sample. **b**, A photograph of a YBCO disk wrapped with carbon fibre fabric and resin-impregnated. The stripes of carbon fibres are clearly visible. The carbon fibre reduced the thermal expansion coefficient, and further enhanced the mechanical strength of the resin.